Large Eddy Simulation Study of Atmospheric Boundary Layer Flow over an Abrupt Rough-To-Smooth Surface Roughness Transition

Kingshuk Mondal
Indian Institute of Technology Hyderabad
K. Naveen Naik
Indian Institute of Technology Hyderabad
K Abhinay
Indian Institute of Technology Hyderabad
Niranjan S Ghaisas (nghaisas@mae.iith.ac.in)
Indian Institute of Technology Hyderabad

Research Article

Keywords:

Posted Date: November 12th, 2022

DOI: https://doi.org/10.21203/rs.3.rs-2229327/v1

Noname manuscript No.
(will be inserted by the editor)

Large Eddy Simulation Study of Atmospheric Boundary Layer Flow over an Abrupt Rough-To-Smooth Surface Roughness Transition

Kingshuk Mondal[1] · K. Naveen Naik[1] · Kondu Abhinay[1] · Niranjan S. Ghaisas[1,2]

Received: DD Month YEAR / Accepted: DD Month YEAR

Abstract
The atmospheric boundary layer flow downstream of an abrupt rough-to-smooth surface roughness transition is studied using large eddy simulations (LES) for a range of surface roughness ratios. Standard wall models assume horizontal homogeneity and are inapplicable for heterogeneous surfaces. Two heterogeneous-surface wall models are evaluated, one based on a local application of similarity theory using a twice-filtered velocity field (BZ model) and another based on a local friction-velocity obtained by blending the upstream and downstream profiles (APA model). The wall shear stress and the turbulence intensity (TI) are sensitive to the wall model while the mean streamwise velocity and the total shear stress (TSS) are less sensitive. The APA model is more accurate than the BZ model on comparison to previous experiments. The APA model results are sensitive to the ratio of the equilibrium and the internal boundary layer (IBL) heights. A value of 0.027 gives good agreement with experiments over a wide range of roughness ratios. The IBL height is insensitive to the turbulent quantity (TSS or TI) on which it is based. Several analytical relations for the IBL height are evaluated using the LES data. Two models are found to be accurate for different roughness ratios while one model is reasonable over the full range investigated. A phenomenological model is

Kingshuk Mondal
E-mail: km1832@me.jgec.ac.in

K. Naveen Naik
E-mail: knaveen1694@gmail.com

Niranjan S. Ghaisas
E-mail: nghaisas@mae.iith.ac.in

[1]Department of Mechanical and Aerospace Engineering, Indian Institute of Technology Hyderabad, Telangana 502284, India

[2]Department of Climate Change, Indian Institute of Technology Hyderabad, Telangana 502284, India

developed for the TI downstream of the roughness jump using a weighted average of the upstream and far-downstream profiles. The model yields reasonable predictions for all roughness ratios investigated.

Keywords Atmospheric boundary layer · Large eddy simulation · Surface heterogeneity · Internal boundary layer · Turbulence intensity

1 Introduction

The atmospheric boundary layer (ABL) is formed in the lowest part of the atmosphere, up to roughly 1 to 3 km above the Earth's surface. The Earth's surface modulates the flow in the ABL through frictional drag, evaporation and transpiration, heat transfer, pollutant emission and terrain induced flow modifications (Stull 1988). The flow critically affects several aspects of human activity ranging from weather, air quality, agriculture to energy extraction from the wind. Land surface is ubiquitously heterogeneous (Bou-Zeid et al. 2020) and the fluxes of momentum, heat, moisture and other passive scalars imposed on the flow depend on the type of land surface. Changes in land characteristics can be due to changing landscapes (e.g. a transition from a water body to land) or due to changing land use (grassland, forest land and cultivated or fallow land). High-fidelity large-eddy simulations (LES) of the ABL flow over heterogeneously rough surfaces forms the topic of the current study.

The momentum fluxes imposed by the ground surface on the ABL flow are often characterized by an 'aerodynamic roughness' (denoted z_0). Such a measure of surface roughness encodes the form drag and skin-friction drag forces imposed by 'sub-surface' roughness elements, or surface irregularities that are much smaller than the ABL height and other length scales over the horizontal directions. Other measures of surface irregularities include the mean height of the irregular features and sand-grain roughness length, commonly denoted as k and k_s, respectively (Abkar et al. 2004). While the three measures can be used interchangeably, the latter two are more commonly used in engineering literature (for $\delta/k < 40$) while the former is commonly used in geophysical studies ($\delta/k > 80$), where δ is the ABL height. In this paper, we restrict attention to the geophysical regime and to a simple configuration wherein the aerodynamic roughness undergoes a step change from a relatively higher value (z_{01}) to a lower value (z_{02}) in the direction that is normal to that of the mean flow.

For an ABL flow over a homogeneously rough surface with aerodynamic roughness z_{01}, without the effects of density stratification, the mean streamwise velocity obeys the logarithmic law of the wall (Stull 1988), the fluctuations of the streamwise velocity follow a reverse logarithmic law (Stevens et al. 2018) and the total vertical shear stress linearly increases from its value at the ground to 0 at the top of the ABL (Bou-Zeid et al. 2004). The expressions for these profiles are

$$\bar{u} = (u_{*1}/\kappa)\ln(z/z_{01}), \tag{1}$$

$$\overline{u'u'} = A - B\ln(z/\delta), \tag{2}$$

$$\overline{u'w'}_{tot} = -u_{*1}^2(1 - z/\delta). \tag{3}$$

Here, u_{*1} is the friction velocity, $\kappa = 0.41$ is the Kármán constant, and A and B are empirical constants, z is the vertical coordinate and δ is the height of the boundary layer. The flow downstream of an abrupt surface roughness transition deviates from these 'equilibrium' conditions. Sufficiently far downstream of the location of the surface roughness transition, a new equilibrium is set up wherein the flow has fully adjusted to the new surface with roughness z_{02}. In the intermediate region, the flow features depend on both, z_{01} and z_{02} (Garratt 1994; Chamorro and Porté-Agel 2009; Efros and Krogstad 2011; Ghaisas 2020).

Early studies on the flow behind an abrupt step change in surface roughness were theoretical in nature. Elliott (1958) proposed a two-layer model of the flow behind an abrupt surface roughness jump, where the lower layer is in equilibrium with the changed surface properties and the upper layer is in equilibrium with the upwind properties. The lower layer which is affected by the new surface was referred to as an 'internal boundary layer' (IBL). The assumption of vertically invariant shear stress within the IBL led to a discontinuity at the height where the IBL meets the undisturbed free flow. This assumption of constant shear stress within the IBL was relaxed in the theory proposed by Panofsky and Townsend (1964) where they assumed the friction velocity to be linearly varying from the ground to the IBL height. Similar two-layer models of the mean velocity were developed by Plate and Hidy (1967) and by Taylor (1969), with different assumptions for the friction velocity or eddy viscosity profiles. In contrast to the two-layer models, a few models have been developed that recognized that the flow downstream of the surface roughness jump that is affected by the changed surface roughness does not immediately attain equilibrium with the new conditions. Such three-layer models (Chamorro and Porté-Agel 2009; Abkar and Porté-Agel 2012; Ghaisas 2020; Li et al. 2022) involve two layers within the IBL, termed the equilibrium boundary layer (EBL) and the transition layer.

Several of the above-mentioned studies require specification of the IBL height as an input. A number of analytical and/or empirical models have in turn been developed for predicting the IBL height, $\delta_i(x)$ as a function of the distance downstream of the surface roughness jump. The Elliott (1958) model is purely empirical but has been widely used as a building block in several further studies. This model as well as the models of Wood (1982) and Jegede and Foken (1999) assume that the IBL height grows as a power-law, $\delta_i \sim x^{0.8}$. The models by Panofsky and Dutton (1984) does not assume a power-law, but proposes an implicit non-linear relation for $\delta_i(x)$ that relies only on the roughness of the downstream surface, z_{02}. A similar implicit relation, but one that involves both the roughness values through its ratio $m = z_{01}/z_{02}$, was proposed by Savelyev and Taylor (2005). It is unclear as to which of these IBL height models is accurate, particularly over a large range of the surface roughness ratio, m. One of the aims of the current study is to use high-fidelity large-eddy simulation data to asses these models for the IBL height.

The above-mentioned theoretical studies mainly focused on modelling the mean streamwise velocity behind an abrupt surface roughness transition. Second-order turbulent quantities, in particular the streamwise turbulence intensity, play a key role in determining fatigue loads on passive structures, such as trees or buildings, and engineering systems, such as solar or wind farms, installed in the ABL. Despite their importance in the design of such objects, analytical models for the streamwise turbulence intensity are largely missing. In this paper, we develop a simple analytical model for the streamwise turbulence intensity downstream of an abrupt surface roughness jump.

Field observations carried out by Bradley (1968) reported velocity profiles and shear stresses downwind of both rough to smooth (RS) and smooth to rough (SR) transitions, which were compared to the predictions made by models of Elliott (1958) and Panofsky and Townsend (1964). Experiments on RS and SR transitions in the engineering domain ($\delta/\kappa < 40$) by Antonia and Luxton (1971, 1972) reported the turbulence intensity and the IBL growth in addition to the velocity and shear stress profiles. Wind tunnel experiments in the geophysical regime have been reported by Chamorro and Porté-Agel (2009) for a RS transition with a surface roughness ratio of 83.3 and by Efros and Krogstad (2011) for a SR transition. Quantities such as the mean velocity profiles, the surace shear stress evolution, profiles of second-order turbulent statistics and the IBL height have been reported in these studies. In particular, the work by Chamorro and Porté-Agel (2009) serves as a good benchmark case for numerical simulations and is used as a reference case for the LES presented in our work.

Several experiments have been reported recently (Hanson and Ganapathisubramani 2016; Li et al. 2019, 2021; Gul and Ganapathisubramani 2022) that are mostly in the engineering domain. These studies have focused on the one- and two-dimensional turbulent spectra and on the integral and smaller length scales in the flow field behind an abrupt roughness transition. Among these studies, one of the cases reported by Li et al. (2021) has a sufficiently large value of δ/k for it to be of geophysical interest. The surface roughness ratio for this case is $m \approx 21.1$, which is significantly different than the $m = 83.3$ (Chamorro and Porté-Agel 2009) data described above. The experimental data reported in Li et al. (2021) case is also used as a benchmark for the LES presented in this paper.

Compared to theoretical studies, field observations and wind tunnel experiments, relatively fewer number of studies have reported numerical simulations of the flow over a surface roughness jump with parameters relevant to the geophysical regime. The works by Shir (1972) and Rao et al. (1974) carried out two-dimensional simulations and used the Reynolds Averaged Navier-Stokes (RANS) technique for turbulence closure. As all the scales of turbulence are modelled instead of being resolved, RANS gives information about only the averaged quantities and is heavily dependent on the model coefficients, making it unreliable for problems involving a surface roughness heterogeneity (Bou-Zeid et al. 2004). In contrast, three-dimensional large-eddy simulations (LES) that resolve the larger scales and model only the smaller scales are better suited for accurately simulating complex turbulent flows over heterogeneous surfaces. A number of LES studies of the flow over heterogeneously rough surfaces with different patterns of surface roughness heterogeneity have been reported, ranging from an infinite number of streamwise-normal stripes (Bou-Zeid et al. 2004), streamwise-aligned stripes with abrupt (Anderson et al. 2015) and gradually varying roughness (Sridhar et al. 2017), oblique stripes (Anderson 2020), and a surface with arbitrarily distributed multi-scale, fractal-like roughness elements (Anderson and Meneveau 2011). In several of these, the roughness features are either fully or partially resolved using a combination of an Immersed Boundary Method (IBM) and sub-surface forcing (Anderson and Meneveau 2010, 2011). The requirement of resolving the near-wall geometry imposes a very high computational cost and restricts several of these studies to the engineering domain, i.e. to Reynolds numbers (based on the free-stream velocity and the boundary layer height) of the order 10^5 to 10^7 and δ/k less than roughly 40.

The primary challenge in LES of the flow over heterogeneous surfaces for very large Reynolds numbers (order 10^{10}) and large δ/k ratios is related to the modelling of the shear stresses very close to the wall. Since the nominal Reynolds numbers are very high for atmospheric flows, a common practice to enable simulations on reasonably-sized grids is to neglect the viscous terms from the Navier-Stokes equations and to introduce an additional stress, $-u_*^2$, at the bottom wall. Here, u_* is a local friction velocity that must be specified as a function of the local flow conditions at every time instant in the simulation. The Monin–Obukhov Similarity theory (MOST) (Monin and Obukhov 1959) has provided the most commonly-used wall model formulation for LES of ABL flows. For neutral conditions, MOST reduces to the law-of-the wall that describes momentum exchange in the surface layer. The logarithmic wind profile in the surface layer predicted by this law-of-the-wall can be inverted to give the friction velocity as $u_* = \langle u \rangle/(\kappa z)$, where $\langle u \rangle$ is the mean streamwise velocity obtained during a simulation at a height z above the ground. This MOST-based wall model is based on the assumption that the flow conditions are statistically identical at all horizontal locations and has been widely adopted in LES of ABL flows (Moeng 1984; Khanna and Brasseur 1997; Brasseur and Wei 2010; Xie et al. 2015; Ghaisas et al. 2017). Since these assumptions of horizontal heterogeneity do not hold for flows involving surface heterogeneities, this model is inappropriate for heterogeneous cases. Two wall models accounting for heterogeneously rough ground surface that provide a way of prescribing the wall shear stress in a localized manner have been proposed in the literature. The wall model by Bou-Zeid et al. (2004), denoted as the 'BZ model' hereafter, is based on filtering the velocity field at a scale larger than the LES-filter width. The wall model by Abkar and Porté-Agel (2012), denoted as the 'APA model', was proposed by recasting a slightly modified diagnostic analytical model of Chamorro and Porté-Agel (2009). This wall model does not require a filtering operation but introduces a so-called blending function that allows for the mean streamwise velocity profile to vary smoothly from its upstream profile to its profile far downstream of the surface roughness jump. The APA model requires specification of the ratio of the equilibrium boundary layer to the internal boundary layer, $\alpha = \delta_e/\delta_i$, as in input parameter.

The APA model has been tested in LES (Abkar and Porté-Agel 2012) for only one value of the surface roughness ratio, $m = 83.3$, and with only one value of $\alpha = 0.027$. Furthermore, the results of Abkar and Porté-Agel (2012) focused only on the mean streamwise velocity profiles and the surface shear stress. Other quantities of interest such as the turbulence intensity, the vertical momentum flux and the internal boundary layer height evolution have not been studied using different heterogeneous-surface wall models in a systematic manner.

This paper describes results of LES of the flow over a heterogeneous surface undergoing an abrupt, rough-to-smooth surface roughness transition using a high-order numerical framework. Our aim is to assess the performance of the BZ and APA wall models by evaluating a range of turbulent statistics beyond only the mean velocity and surface shear stress. A second aim is to study the sensitivity of the APA model results to the input parameter $\alpha = \delta_e/\delta_i$, or the ratio of the equilibrium and internal boundary layer heights. We also report simulation results for different roughness ratios, $m = z_{01}/z_{02}$. Several previously developed models for the IBL height are evaluated using our LES results. Finally, a phenomenological model is proposed for the turbulence intensity profile downstream of a step change in surface roughness.

The numerical methodology and cases studied are described in Sect. 2. Details of the wall models that are assessed here are given in Sect. 2.2. Results are presented and discussed in Sect. 3 and conclusions are presented in Sect. 4.

2 Numerical Methodology

2.1 LES Methodology

LES is employed to simulate the boundary layer flow over a surface with an abrupt change in surface roughness. The incompressible, LES-filtered Navier-Stokes (NS) equations that are solved can be written as

$$\frac{\partial \tilde{u}_i}{\partial x_i} = 0 \tag{4}$$

$$\frac{\partial \tilde{u}_i}{\partial t} + \frac{\partial}{\partial x_j}\left(\tilde{u}_i \tilde{u}_j\right) = -\frac{1}{\rho}\frac{\partial \tilde{p}}{\partial x_i} - \frac{\partial \tau_{ij}}{\partial x_j} + f_i \tag{5}$$

where $\tilde{u}_i$ is the instantaneous resolved velocity in i-direction, t is the time, and x_i with $i = 1, 2$ and 3 are the three Cartesian coordinate directions which can be used interchangeably with x, y and z. The filtered pressure field is denoted by $\tilde{p}$ and ρ is the (constant) density of air.

The tensor τ_{ij} is usually comprised of the viscous stresses ($-2\nu\tilde{S}_{ij}$, where ν is the viscosity and $\tilde{S}_{ij}$ is the strain-rate tensor) and the subgrid scale (SGS) stresses ($\tau_{ij}^{sgs} = \widetilde{u_i u_j} - \tilde{u}_i\tilde{u}_j$). However, the nominal Reynolds number based on the free-stream velocity, the height of the boundary layer and the viscosity of air is of the order 10^{10} in atmospheric flows. As a result, the direct effects of viscosity are negligible over most of the domain except for a very thin region close to the bottom surface. The effects of these extremely thin viscous sub-layer and transition layer are modelled through a wall model and the viscous terms are neglected over the entire domain. The tensor τ_{ij} is thus comprised of the SGS stresses and the wall stresses, $\tau_{ij} = \tau_{ij}^{sgs} + \tau_{ij}^{wm}$.

The Anisotropic Minimum Dissipation (AMD) model, introduced by Rozema et al. (2015), is used to model the effect of the subgrid scales on the larger, filtered, scales of motion. The trace of the SGS stress tensor is incorporated along with the pressure while the deviatoric part is given by $\tau_{ij}^{sgs,d} = \tau_{ij}^{sgs} - (\tau_{kk}^{sgs}/3)\delta_{ij} = -2\nu_{sgs}\tilde{S}_{ij}$, with the eddy viscosity ν_{sgs} given by the AMD model. This model has been extensively tested previously for a variety of flow configurations including simulations of atmospheric boundary layers and turbulent channels (Rozema et al. 2015; Abkar et al. 2016; Vreugdenhil and Taylor 2018; Zahiri and Roohi 2019; Ghaisas et al. 2020). The wall stresses, τ_{ij}^{wm}, are prescribed as discussed in detail in the next section.

The above-mentioned equations are solved using the concurrent precursor simulation method (Stevens et al. 2014). This methodology is similar to the one explained in detail in Ghaisas et al. (2020). Two computational domains of sizes ($L_x \times L_y \times L_z$) each are used. The first, 'precursor', domain is driven by an imposed constant pressure gradient, $f_i = -u_{*1}^2/L_z$, and has a homogeneous surface roughness, z_{01}. u_{*1} denotes the equilibrium friction velocity. A shifted periodic boundary condition (Munters et al. 2016) is applied to the precursor domain to ensure that spurious, infinitely long, streamwise-aligned streaks do not develop in the domain and contaminate the solution. The second, 'main', domain (see Fig. 1) has an upstream portion with aerodynamic roughness z_{01}, followed by a transition to a surface with roughness z_{02}. The last portion of the main domain is a 'fringe' region, wherein the flow is nudged towards the same upstream conditions as in the precursor domain using the additional forcing term f_i. The surface roughness in the fringe region is the same as in the upstream and precursor domains, i.e. z_{01}. The top boundary ($z = L_z$) is imposed with no-penetration, free-slip conditions and all the horizontal (x, y) boundaries are periodic. The bottom boundary is a no-penetration wall, and a shear stress is applied using a wall model.

The 'PadeOps-igrid' code (Subramaniam et al. 2021) developed over the years is used for the simulations. This code uses Fourier-spectral discretization in the horizontal (x, y) directions, 6^{th}-order staggered compact finite-difference scheme in the vertical (z) direction and a 3^{rd}-order Runge-Kutta method for time advancement. The code is well validated and has been used previously

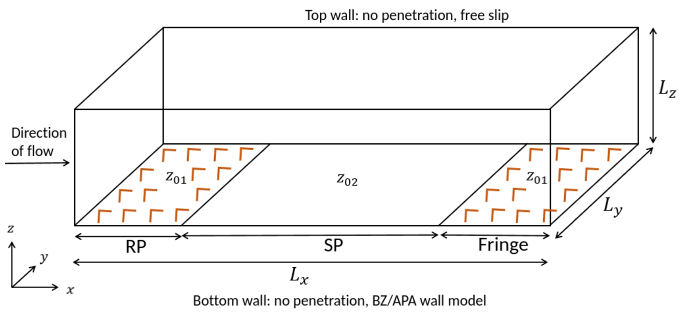

Fig. 1 Schematic of the 'main' domain showing different dimensions of the computational domain. Boundary conditions for the top and bottom wall are shown. z_{01} and z_{02} are the aerodynamic roughness for the rough surface and the smooth surface respectively. The fringe region has the same roughness as the upwind of the step jump; RP stands for rough patch, SP stands for smooth patch

for several problems including rough-wall turbulent channels (Ghate and Lele 2020), stratified and unstratified atmospheric boundary layers (Ghate and Lele 2017), and problems involving wind turbines or farms (Ghate et al. 2020; Ghaisas et al. 2020; Howland et al. 2020).

2.2 Wall Models

The effect of viscosity is modelled by introducing the term τ_{ij}^{wm} in the total stress in the Navier-Stokes equations. Since viscous effects are important only close to the wall, τ_{ij}^{wm} is zero at all points in the domain except at the bottom wall, $z = 0$. Furthermore, only the vertical shear components (i.e. τ_{i3}^{wm} with $i = 1, 2$) are non-zero.

The standard 'equilibrium' wall model based on the Monin-Obhukhov Similarity Theory (Moeng 1984) first estimates the magnitude of the mean shear stress ($-\langle u_* \rangle^2$) by inverting the logarithmic law-of-the-wall. The horizontally-averaged streamwise velocity ($\langle \tilde{u}_1 \rangle$) available during the LES at the first grid point from the wall (i.e. $z = \Delta z/2$) is used in these models to determine the mean shear stress. The mean shear stress is then distributed into its two components, i.e. τ_{13}^{wm} and τ_{23}^{wm}, with each component being proportional to the corresponding component of the instantaneous local filtered horizontal velocity,

$$\tau_{i3}^{wm}(x, y, 0) = -\langle u_* \rangle^2 \frac{\tilde{u}_i}{\left(\tilde{u}_1^2 + \tilde{u}_2^2\right)^{1/2}}, \quad \langle u_* \rangle = \frac{\langle u_1(\Delta z/2) \rangle \, \kappa}{\ln(\Delta z/2 z_0)}. \tag{6}$$

Here, $\langle .. \rangle$ denotes a horizontal averaging operation. This model is inapplicable for flows over heterogeneously rough surfaces since it is inappropriate to carry out a horizontal average in such flows. A few studies tried to overcome this problem by applying the logarithmic law-of-the-wall in a strictly local sense

(Albertson and Parlange 1999). However, it is easily shown, using the Cauchy-Schwartz inequality, that this leads to an over-prescription of the wall shear stress.

Two previously-proposed wall models that try to account for non-equilibrium effects induced by the presence of the surface roughness step are evaluated in this paper. These models are described next.

The first model evaluated here was proposed by Bou-Zeid et al. (2004) and is denoted as the 'BZ' wall model in this paper. This strictly local wall model uses a velocity field that is filtered using a width of size 2Δ, where $\Delta = (\Delta x \Delta y \Delta z)^{1/3}$ is the characteristic grid size. Referring to this velocity field filtered at the 2Δ-scale as $\widehat{\widetilde{u}}_i$, the wall shear stress is given by

$$\tau_{i3}^{wm}(x,y,0) = -[u_*(x,y)]^2 \frac{\widehat{\widetilde{u}}_i(x,y,\Delta z/2)}{\sqrt{\widehat{\widetilde{u}}_1(x,y,\Delta z/2)^2 + \widehat{\widetilde{u}}_2(x,y,\Delta z/2)^2}}, \tag{7}$$

where the local friction velocity is given by assuming that the $2\Delta-$filtered horizontal velocity satisfies the law-of-the-wall locally,

$$u_*(x,y) = \frac{\kappa}{\ln[\Delta z/2z_0(x,y)]} \sqrt{\widehat{\widetilde{u}}_1(x,y,\Delta z/2)^2 + \widehat{\widetilde{u}}_2(x,y,\Delta z/2)^2}. \tag{8}$$

In this study, $z_0(x,y)$ is either z_{01} or z_{02} depending on the roughness of the underlying surface at the horizontal location given by coordinates (x,y). This model reduces the over-prescription of the mean wall shear stress since the $2\Delta-$filtered velocity field has much smaller fluctuations. This model also does not require a horizontal averaging operation and hence can be applied to heterogeneously rough surfaces.

The second wall model evaluated here is that originally proposed by Chamorro and Porté-Agel (2009) and modified by Abkar and Porté-Agel (2012). We denote this as the 'APA' model. This model uses the same formulation as Eq. 7 but it does not rely on the assumption that the local friction velocity satisfies a local logarithmic law-of-the-wall immediately downstream of an abrupt surface roughness transition. Instead, this model explicitly accounts for the fact that the local friction velocity changes along the streamwise direction and gradually approaches its equilibrium value by using a blending function $\lambda(x,z)$. The local friction velocity is given by

$$u_{*2}(x) = \frac{\kappa}{\ln(\Delta z/2z_{02})} \frac{[\overline{\widehat{\widetilde{u}}_1}(x,\Delta z/2) - \lambda(x,\Delta z/2)\frac{u_{*1}}{\kappa}\ln(\Delta z/2z_{01})]}{[1-\lambda(x)]}, \tag{9}$$

Here, $\overline{(..)}$ denotes averaging in the spanwise (y) direction. u_{*1} is the friction velocity in the upstream region, which is also the friction velocity in the precursor domain since the flow in the upstream region is driven by the flow in the precursor domain. The blending function is modelled as $\lambda(x,z) = \ln[z/\delta_e(x)]/\ln[\delta_i(x)/\delta_e(x)]$, and is evaluated at $x = \Delta z/2$ in Eq. 9. Here, $\delta_i(x)$

is the height of the internal boundary layer (IBL) at a distance x from the location of the abrupt transition in surface roughness. The IBL height is specified using the empirical relation proposed by Elliott (1958),

$$\delta_i(x) = z_{02}\left[0.75 - 0.03\ln\left(\frac{z_{02}}{z_{01}}\right)\right]\left(\frac{x}{z_{02}}\right)^{0.8}. \tag{10}$$

In this equation, $\delta_e(x)$ is the equilibrium boundary layer height and was assumed by Abkar and Porté-Agel (2012) to be a constant fraction of the IBL height, $\delta_e(x) = \alpha\,\delta_i(x)$. This model is applicable only in the region where the surface roughness has abruptly changed from its upstream value to z_{02} because $\lambda < 1$ in this region. The value of λ is set to zero once the equilibrium boundary layer crosses the first computational grid point, i.e. once $\delta_e(x) > \Delta z/2$. Beyond this streamwise location, the model reduces to the BZ model with the surface roughness equal to z_{02}.

In the entirety of the precursor domain, in the portion of the main domain that is upstream of the abrupt surface roughness transition, and in the fringe portion of the main domain where the flow is nudged towards the same flow field as in the precursor domain, the surface roughness is uniformly z_{01}. In these three regions, the BZ wall model with surface roughness equal to z_{01} is applied. In the portion of the main domain between the abrupt transition and the fringe, either the BZ model (Eqs. 7 and 8) with roughness z_{02} or the APA model (Eqs. 7 and 9) is applied. We refer to these two combinations as 'BZ' model and 'APA' model respectively.

2.3 Cases Simulated

The computation domain dimensions are selected as per the experiments reported by Chamorro and Porté-Agel (2009), $(L_x, L_y, L_z) = (3.84, 0.64, 0.4)$ m. The origin of the coordinate system is placed at the location of the roughness jump which is situated at 0.96 m from the left end of the domain. The upstream surface aerodynamic roughness height is $z_{01} = 0.5$ mm, as used by Chamorro and Porté-Agel (2009). The downstream surface has different roughness values as described below. All spatial dimensions are normalized by 0.4/3 m so that the vertical height of the domain, which is 0.4 m in the experiments of Chamorro and Porté-Agel (2009), becomes 3 non-dimensional units. Figure 2 shows the different portions of the computational domain in scaled units.

A total of nineteen LES simulations are carried out. The cases are selected so as to cover different roughness ratios ($m = z_{01}/z_{02}$), wall models, different grid sizes and different values of the parameter $\alpha = \delta_e/\delta_i$ which is an input to the APA model.

First, a set of six simulations for $m = 83.3$ covers the two wall models (BZ and APA) discussed in the preceding section and three grid sizes comprised of $128 \times 32 \times 32$ (G1), $192 \times 64 \times 64$ (G2) and $240 \times 80 \times 80$ (G3) points. It should be noted that this number of points is used to discretize each of the two

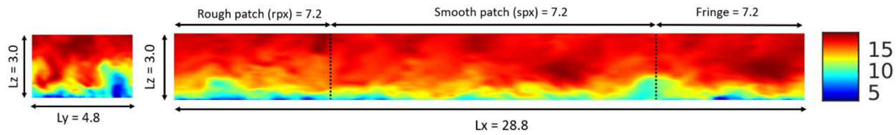

Fig. 2 Contours of the streamwise velocity at an arbitrary time instant from a $240 \times 80 \times 80$ simulation for $m = 83.3$ using the BZ wall model. Dimensions of the main computational domain in the (a) $y - z$ plane and (b) $x - z$ plane are shown. Upstream rough patch, surface roughness step, downstream smooth patch and the fringe region are also marked

Table 1 Summary of cases simulated. Cases 1 to 16 have a surface roughness transition from $z_{01} = 0.5$ mm to z_{02} at $x = 0$ in the main domain and surface roughness is z_{01} everywhere in the precursor domain. Cases number 17 to 19 are homogeneously rough with the mentioned z_0 in both domains. Number of grid points mentioned are per domain. Actual number of points used in each simulation is twice that mentioned below.

Case No.	Grid	Wall Model	$m = z_{01}/z_{02}$	$\alpha = \delta_e/\delta_i$	z_{02} (mm)
1	$240 \times 80 \times 80$	BZ	83.3	-	0.006
2	$240 \times 80 \times 80$	APA	83.3	0.027	0.006
3	$192 \times 64 \times 64$	BZ	83.3	-	0.006
4	$192 \times 64 \times 64$	APA	83.3	0.027	0.006
5	$128 \times 32 \times 32$	BZ	83.3	-	0.006
6	$128 \times 32 \times 32$	APA	83.3	0.027	0.006
7	$240 \times 80 \times 80$	BZ	20	-	0.025
8	$240 \times 80 \times 80$	APA	20	0.027	0.025
9	$240 \times 80 \times 80$	BZ	125	-	0.004
10	$240 \times 80 \times 80$	APA	125	0.027	0.004
11	$240 \times 80 \times 80$	APA	20	0.054	0.025
12	$240 \times 80 \times 80$	APA	20	0.108	0.025
13	$240 \times 80 \times 80$	APA	83.3	0.054	0.006
14	$240 \times 80 \times 80$	APA	83.3	0.108	0.006
15	$240 \times 80 \times 80$	APA	125	0.054	0.004
16	$240 \times 80 \times 80$	APA	125	0.108	0.004
17	$240 \times 80 \times 80$	BZ	1	-	$z_0 = 0.025$ mm everywhere
18	$240 \times 80 \times 80$	BZ	1	-	$z_0 = 0.006$ mm everywhere
19	$240 \times 80 \times 80$	BZ	1	-	$z_0 = 0.004$ mm everywhere

domains per simulation, so that the actual number of computational points in each simulation is twice that mentioned above and in Table 1.

The second set of simulations covers two additional values of $m = 20$ and 125 and the two wall models. Following a grid sensitivity study, we use the finest grid (G3) for the four runs in this set.

In all the cases mentioned above that involve the APA wall model, the value of $\alpha = 0.027$ is used, where $\alpha = \delta_e/\delta_i$, is the ratio of the equilibrium to the internal boundary layer height. To study the sensitivity to this input parameter, six additional cases using the APA model, with $\alpha = 0.054$ and 0.108, for the three surface roughness ratios ($m = 20, 83.3, 125$) on the G3 grid are carried out.

Finally, simulations over homogeneously rough surfaces with the tabulated roughness values are conducted. These cases are useful for developing an analytical model for the turbulence intensity described later in this paper.

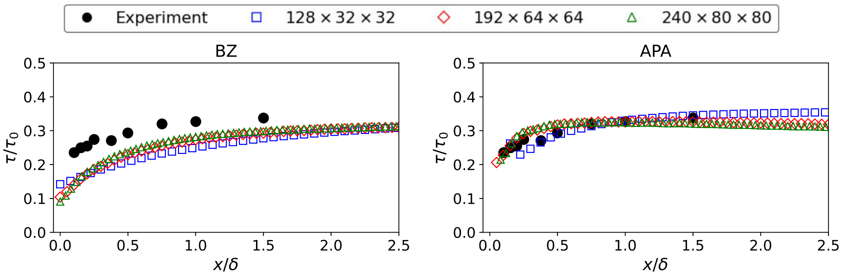

(a) (b)

Fig. 3 Streamwise evolution of wall shear stress after the abrupt surface roughness transition for different grid sizes using (a) BZ and (b) APA wall models. Experimental results are from Chamorro and Porté-Agel (2009)

The upstream friction velocity is $u_{*1} = 0.5473$ m/s following Chamorro and Porté-Agel (2009). All the simulations are carried over 100 non-dimensional time units (normalized using $\delta_{exp} = 0.4$ m and u_{*1} as reference scales). Statistical averaging is performed over the last 60 time units. Averaging is performed in time and along the horizontal (x, y) directions for the precursor domain and over time and the spanwise (y) direction in the main domain.

3 Results & Discussion

3.1 Grid Convergence

Sensitivity of different statistics of the ABL flow to the grid resolution used in the LES are studied first. Besides using two wall models and three different grids, the results are also compared with experimental data of Chamorro and Porté-Agel (2009) wherever available.

Figure 3 shows the surface shear stress after the change in surface roughness for different grid sizes using the BZ and APA wall models for $m = 83.3$. Here, the shear stress at the bottom wall downstream of the surface roughness jump (τ) is normalized by the surface shear stress upstream of the jump (τ_0). The LES data show appreciable change in magnitude when compared between the $128 \times 32 \times 32$ and $192 \times 64 \times 64$ grid cases. An additional simulation for grid size of $240 \times 80 \times 80$ is also compared and it is observed that there is little change in magnitudes when compared with the $192 \times 64 \times 64$ grid.

The temporally and spanwise averaged streamwise velocities at two downstream locations $(x/\delta = 0.5,\ 1.0)$ after the roughness jump are presented in Fig. 4. These profiles are almost insensitive to the grid resolution for both models. Small differences are seen close to the top of the domain, where the velocity profiles are seen to agree better with the upstream logarithmic 'law of the wall' profile, Eq. 1, with increasing grid resolution. Closer to the bottom boundary, the velocity accelerates due to the reduced surface roughness. This acceleration is the same for all grids for the BZ as well as APA wall models.

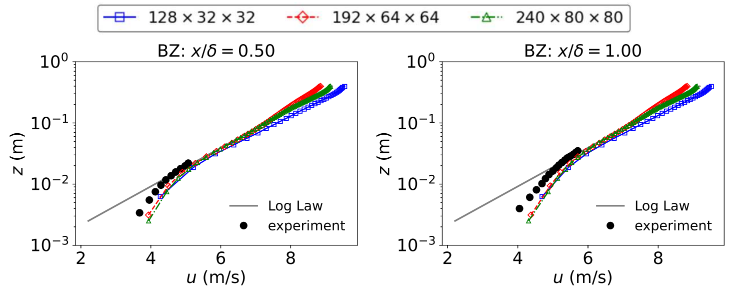

(a)

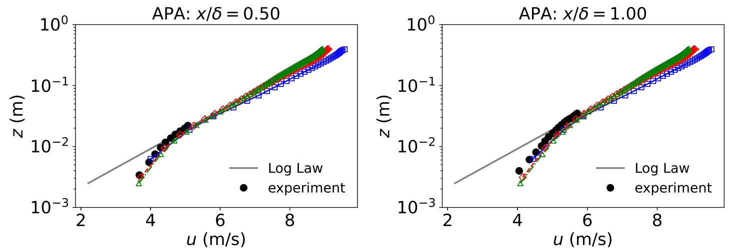

(b)

Fig. 4 Vertical profiles of the mean streamwise velocity at different downstream locations after the abrupt surface roughness transition for different grid sizes for $m = 83.3$ using (a) BZ and (b) APA wall models

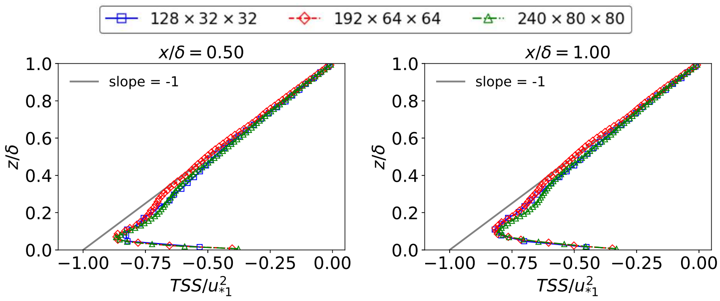

(a) TSS

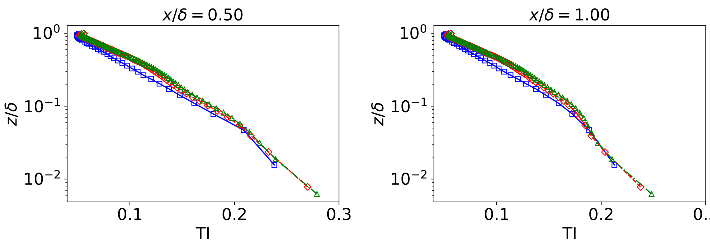

(b) TI

Fig. 5 Vertical profiles of (a) TSS and (b) TI at different downstream locations after the roughness jump using different grid sizes and the APA wall model for $m = 83.3$

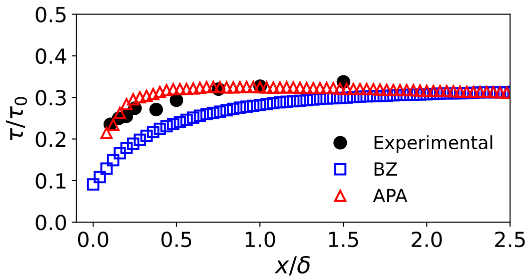

Fig. 6 Streamwise evolution of wall shear stress for $m = 83.3$ on grid G3 using BZ and APA wall models compared to the experimental data of Chamorro and Porté-Agel (2009)

The streamwise turbulence intensity (TI) and the total shear stress (TSS) are shown at the same downstream locations as the streamwise velocity for the APA wall model in Fig. 5. The TSS has contributions due to the resolved scales, subgrid scales and the wall model i.e. $TSS = \overline{u'w'} + \overline{\tau_{13}^{sgs}} + \overline{\tau_{13}^{wm}}$. The TSS profiles are almost independent of the number of grid points employed. The turbulence intensity is defined as the ratio of the standard deviation of the streamwise velocity to the mean velocity,

$$TI = \sqrt{\overline{u'u'}}/\overline{u}. \quad (11)$$

The TI increases when going from the coarsest to the intermediate grid, but is unchanged over the two finest grids employed here. This indicates that a computational grid with $240 \times 80 \times 80$ points is sufficient to obtain grid-independent results. All subsequent simulations utilize these many grid points.

3.2 Sensitivity of ABL Statistics to Wall Models

Sensitivity of the results to the wall model employed is studied next.

Following the surface roughness jump at $x = 0$, the shear stress applied by the new smooth surface on the flow is smaller compared to that applied by the upstream rough surface. The wall shear stresses obtained from the LES runs of different wall models are compared to the experimental data of Chamorro and Porté-Agel (2009) in Fig. 6. It is seen that the BZ model under-predicts the wall shear stress values while the APA wall model results agree well with the experimental results. Furthermore, Fig. 3 shows that, on refining the grid, the values converge towards the experimental results for both models. The convergence is monotonic in case of BZ, but quite slow. This indicates that the BZ model would yield good agreement with the experiments on a very refined mesh.

The LES results using the APA model are in much better agreement with the experimental results than those using the BZ model. This is true for all grid sizes studied, but the convergence is not monotonic (see Fig. 3). A careful inspection of Fig. 6 shows that the computed shear stress values using the

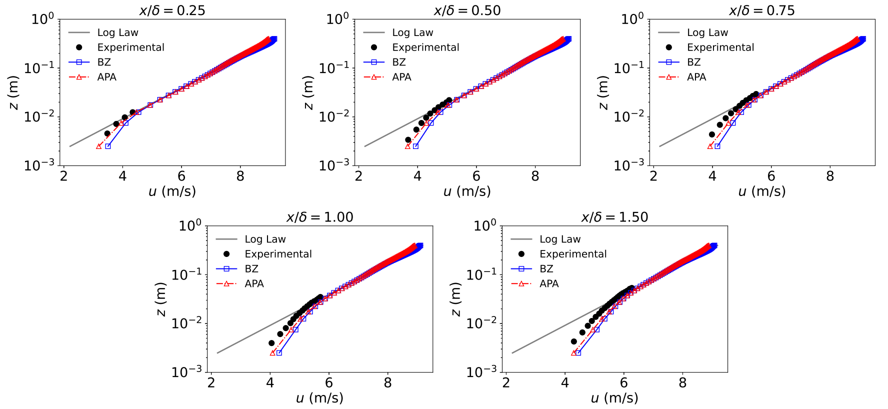

Fig. 7 Vertical profiles of mean streamwise velocity at different locations downstream of the abrupt surface roughness transition on grid G3 for $m = 83.3$ using different wall models

APA model reduce slightly between $x/\delta = 0.5$ and $x/\delta = 1.5$. As discussed later, in Sect. 3.3, this feature is absent for larger values of the ratio $\alpha = \delta_e/\delta_i$.

Figure 7 compares the upstream logarithmic law-of-the-wall profile, the experimental results (Chamorro and Porté-Agel 2009) and the mean velocity profiles obtained from the LES on the finest grids using the two wall models at several locations downstream of the roughness jump for $m = 83.3$. It is clear that the LES results adhere to the law-of-the-wall closely above a certain height. This height above which the downstream and upstream profiles are identical is called the internal boundary layer (IBL) height and is discussed in detail later. Below the IBL height, the APA model results are in slightly better agreement with the experimental results than the BZ model results. This is consistent with the under-predictions of the surface shear stresses found in Fig. 6.

Vertical profiles of TSS obtained from different regions of the simulation domains are shown in Fig. 8. For a fully-developed statistically stationary turbulent boundary layer in a half-channel, the TSS normalized by its value at the bottom wall (u_{*1}^2) is expected to follow a slope of -1 reducing in magnitude from 1 at the wall to 0 at the top (Eq. 3). The profile obtained from averaging over the precursor domain (surface roughness z_{01} everywhere) agrees very well with this theoretically expected line. The profile obtained by averaging over the upstream portion of the main simulation domain (before $x = 0$ with surface roughness z_{01}) also agrees well with this theoretically expected line.

The profiles of TSS averaged over the spanwise coordinate at different locations downstream of the surface roughness jump ($x > 0$) are found to be insensitive to the wall model. Close to the bottom wall, the magnitude of the TSS is smaller compared to its upstream value, consistent with the axial evolution of the surface shear stress shown in Fig. 6 and with the fact that the surface roughness reduces at $x = 0$, i.e. $z_{02} < z_{01}$. Furthermore, it is seen that the TSS varies linearly from its value at the wall to the top of the IBL

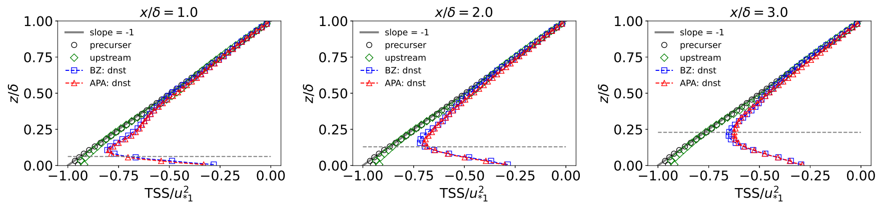

Fig. 8 Vertical profiles of TSS at different locations downstream of the abrupt surface roughness transition on grid G3 for $m = 83.3$ using different wall models. The grey dashed line represents the IBL height at each x/δ location and 'dnst' stands for downstream.

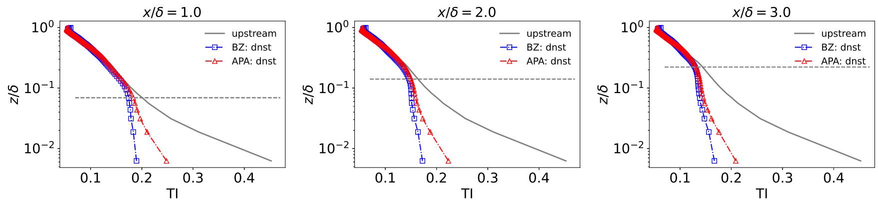

Fig. 9 Vertical profiles of TI at different locations downstream of the abrupt surface roughness transition on grid G3 for $m = 83.3$ using different wall models. The grey dashed line represents the IBL height at each x/δ location and 'dnst' stands for downstream.

(marked by dashed gray lines). This indicates that several early analytical models (Panofsky and Townsend 1964; Chamorro and Porté-Agel 2009) were based on an incorrect assumption of constant shear stress within the IBL, but supports the assumption made in a recent analytical model by Ghaisas (2020).

Unlike the TSS, the TI downstream of the step is very much sensitive to the wall models as shown in Fig. 9. The profile upstream of the roughness jump has larger values of TI close to the wall, once again consistent with the fact that the configuration being studied is a rough-to-smooth surface transition, or $z_{02} < z_{01}$. The TI value at the wall obtained using the APA model is larger than that obtained using the BZ model, consistent with the surface shear stresses obtained using these two wall models (see Fig. 6). In each panel of Fig. 9, the influence of the changed roughness on the downstream profiles is seen to be prominent near the wall but it disappears after a certain height similar to the mean velocity profiles. This again indicates the presence of an IBL within which the effects of the changed surface roughness are confined.

To study the evolution of the internal boundary layer, the IBL heights extracted from the LES data based on two turbulent statistics, TSS and TI, are presented in Fig. 10. The dashed vertical line marks the jump in aerodynamic roughness from rough to smooth. For each profile, the IBL height is determined as the smallest distance from the bottom wall where the upstream and downstream profiles differ by less than 10%. The IBL profiles for both TSS and TI are insensitive to the wall models as seen from Figs. 10a and 10b. Also, it is evident from Fig. 10c that the IBL based on TSS profiles are similar to

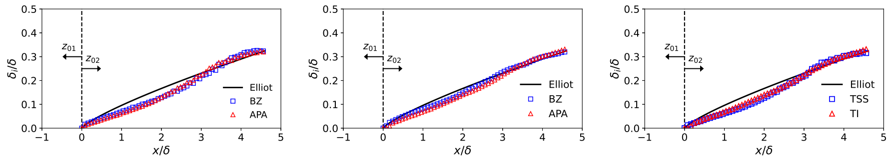

(a) (b) (c)

Fig. 10 Streamwise evolution of the height of the internal boundary layer for $m = 83.3$ based on (a) TSS and (b) TI using the two wall models. (c) Comparison of IBL heights based on the two turbulent statistics using the APA wall model. Symbols denote LES data using grid G3. Lines denote predictions of the empirical model of Elliott (1958)

those based on TI profiles. Finally, the empirical relation proposed by Elliott (1958), Eq. 10, for the IBL height is seen to be quite accurate for $m = 83.3$.

3.3 Sensitivity of APA wall model to the ratio of internal and equilibrium boundary layer heights

As discussed in Sect. 2.2, the ratio of the equilibrium boundary layer height (δ_e) to the internal boundary layer height (δ_i), i.e. $\alpha = \delta_e/\delta_i$, is an input parameter to the APA model. We study the sensitivity of the APA model LES results to this parameter by considering three different values of $\alpha = 0.027$, 0.054 and 0.108. This sensitivity is studied for three values of surface roughness ratios, $m = z_{01}/z_{02} = 25$, 83.3 and 125. The upstream roughness z_{01} is kept unchanged and the downstream roughness is altered in three cases to get $m = 20$, 83.3 and 125. A total of nine LES are analyzed in this subsection.

Fig. 11a shows the streamwise evolution of the wall shear stress for the different cases. For $m = 83.3$ the results are compared with the experimental data (Chamorro and Porté-Agel 2009). The $m = 20$ LES results are compared to the experimental data at a slightly different value of $m \approx 21.1$ reported by Li et al. (2021). Due to lack of experimental data for the last case, RANS simulations by Shir (1972) are used for comparison.

The wall shear stresses obtained from the LES using the APA wall model are clearly sensitive to the parameter α. This is contrary to what was suggested, but not explicitly shown, in the study of Abkar and Porté-Agel (2012). For $m = 20$ as well as $m = 83.3$, the agreement with the experimental results is the best for $\alpha = 0.027$. This is seen more quantitatively in Table 2, where the L_2 norms of the relative errors, expressed as a percentage, are shown. The tabulated values are calculated as

$$\epsilon = \sqrt{\frac{1}{N}\sum_{i=1}^{N}\left(\frac{\tau - \tau_{\text{exp}}}{\tau_0}\right)^2} \times 100, \tag{12}$$

where N is the number of measurement points. The error norms are smallest for $\alpha = 0.027$ for both $m = 20$ and 83.3. The value $\alpha = 0.027$ was recommended by Abkar and Porté-Agel (2012) and is found to be appropriate

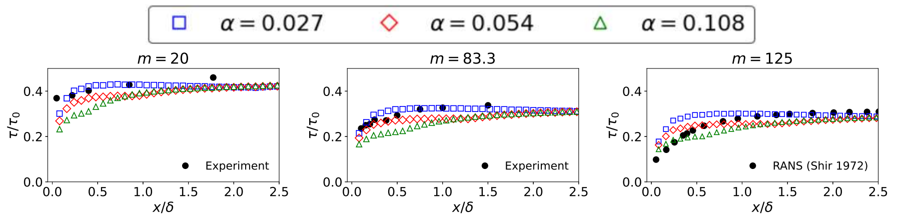

(a) Surface shear stress

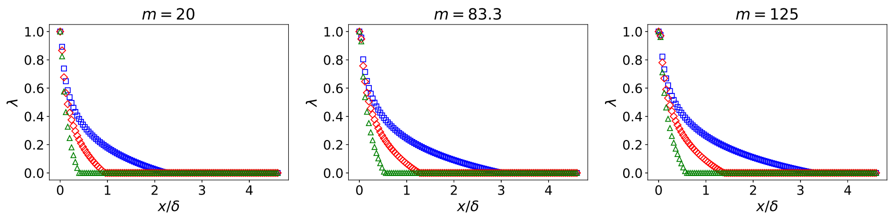

(b) Blending function

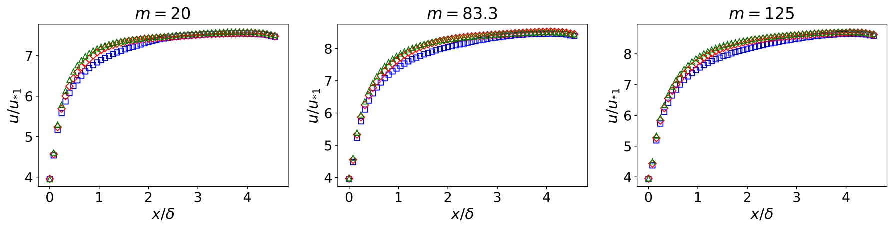

(c) Streamwise velocity at first grid point from the wall

Fig. 11 Streamwise evolution of (a) wall shear stress (b) λ and (c) mean streamwise velocity at $z = \Delta z/2$ computed for different roughness ratios m using the APA model with different values of α on grid G3. In panel (a) the experimental data are from Li et al. (2021) for $m = 20$ and from Chamorro and Porté-Agel (2009) for $m = 83.3$. The RANS data for $m = 125$ are from Shir (1972)

Table 2 Error norms between the surface shear stress values obtained from LES and from previous experiments, calculated using Eq. 12, for different α and m values.

$m = z_{01}/z_{02}$	$\alpha = 0.027$	$\alpha = 0.058$	$\alpha = 0.108$
20	2.14%	4.35%	7.9%
83.3	2.12%	3.21%	6.21%

over a range of m values with the current numerical framework involving a high-order compact finite-difference scheme in the vertical direction.

The LES results for $m = 125$ are in fair agreement with the RANS results. However, due to the strong assumptions involved in RANS models, these cannot be used as a benchmark to assess LES simulation results. However, the value of $\alpha = 0.027$ is likely to be appropriate for values of m beyond 83.3 as well, although this needs to be confirmed by future experiments or wall-resolved DNS or LES simulations.

Fig. 11a also shows that the surface shear stress values attained far downstream of the transition are independent of the value used for α. To understand the behaviour of the APA wall model in the intermediate region further, profiles of the blending function, $\lambda(x, \Delta z/2)$, and the spanwise-averaged velocity at the first off-wall grid point, $\overline{u}_1(x, \Delta z/2)$, are shown in Figs. 11b and 11c. An increase in α leads to a significant decrease in λ for a given x, consistent with the model used for λ. In other words, increasing the α leads to the λ profile approaching its far-downstream value of 0 faster. In conjunction with Eq. 9, this would at first suggest that the surface shear stress approaches its far-downstream value at a smaller x location for a larger value of α. Figure 11 however shows the opposite is true, namely the surface shear stress approaches its far-downstream value faster for smaller α. This is explained by the small differences in the evolution of the streamwise velocity at the first off-wall grid point (Fig. 11b) due to different α values.

Other statistics such as streamwise velocity, TSS and TI are plotted for different m and α values in Fig. 12. Except for small differences for different values of α for $m = 20$, these quantities are mostly insensitive to α.

3.4 Sensitivity to roughness ratio

Sensitivity to the roughness ratio is studied by analysing simulation results for $m = 20, 83.3$ and 125. The APA wall model with $\alpha = 0.027$ is used for all the runs.

Figure 13a shows that for a configuration with smaller roughness ratio, the shear stress downstream of the surface roughness jump is larger. This is consistent with intuition since a smaller $m = z_{01}/z_{02}$ for the same z_{01} implies a downstream surface that exerts more resistance to the flow. The change in the downstream surface shear stress between $m = 83.3$ and 125 is smaller than that between $m = 20$ and 83.3. This suggests that the downstream surface shear stresses will asymptotically approach limiting values for higher values of m.

Due to smaller wall shear stress for higher m values, the flow accelerates faster after the roughness jump as seen in Fig. 14a. It is observed that for the largest two values of m studied here, the change in $\overline{\tilde{u}}$ is insignificant. The same trends are seen to hold for the TSS and TI profiles (Figures 14b and 14c, respectively). A lower value of m indicates a rougher surface after the step jump, which increases the turbulent statistics in the flow. As a result, TSS and TI have larger magnitudes within the IBL for smaller values of m. Similar to $\overline{\tilde{u}}$, the changes in TSS and TI are insignificant between $m = 83.3$ and 125. Finally, Fig. 13b shows that the IBL height evolution is very similar for all three surface roughness ratios.

Several analytical models (Panofsky and Townsend 1964; Chamorro and Porté-Agel 2009; Ghaisas 2020) for the mean velocity downstream of a surface roughness jump as well as the APA wall model require the internal boundary layer height as an input. A number of empirical and/or physics-based models

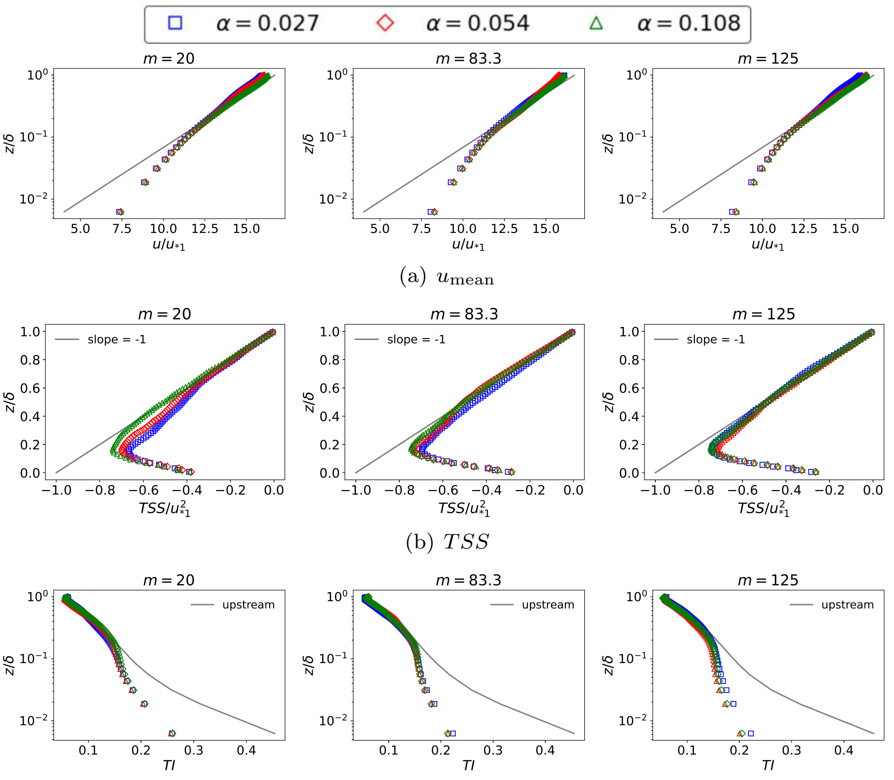

(a) u_{mean}

(b) TSS

(c) TI

Fig. 12 Vertical profiles of (a) mean streamwise velocity, (b) TSS and (c) TI for different roughness ratios m using different α in the APA model at the downstream location of $x/\delta = 2.0$ on grid G3

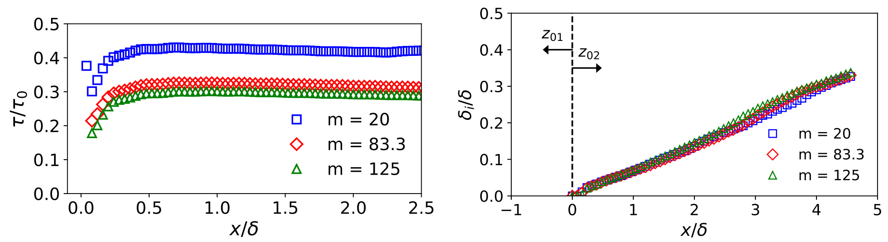

(a)

(b)

Fig. 13 Streamwise evolution of (a) wall shear stress and (b) IBL height based on the turbulence intensity from LES using the APA wall model for different roughness ratios on grid G3

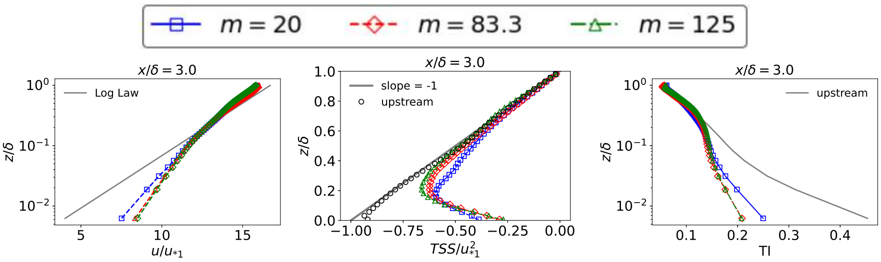

(a) u_{mean} (b) TSS (c) TI

Fig. 14 Vertical profiles of (a) mean streamwise velocity, (b) TSS and (c) TI at a downstream location of $x/\delta = 3.0$ for different m values using the APA wall model on grid G3

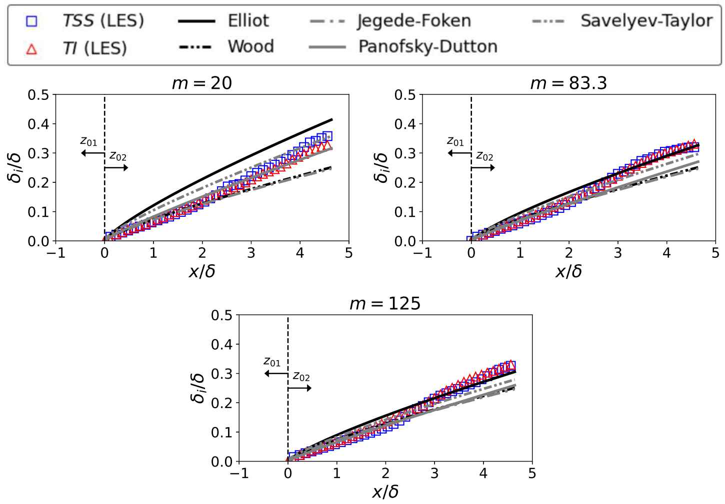

Fig. 15 Comparison of IBL heights obtained from LES (based on TSS and TI) to predictions of five IBL models listed in Table 3 for different m values using the APA model on grid G3

have in turn been developed for the IBL height. Fig. 15 compares the IBL height obtained from the LES using the APA wall model with predictions of five different IBL models. A quantitative assessment of the errors between the LES results and the IBL model predictions is shown in Table 4. Details of the models evaluated here are given in Table 3. Some of these models require the solution of a nonlinear equation which is achieved using the 'fsolve' function in Matlab. The prediction of the Elliott (1958) model serves as a good starting guess for the root-finding procedure at each x.

The models by Wood (1982) and by Jegede and Foken (1999) agree with the LES results till about $x/\delta \approx 2.5$ but under-predict the LES results beyond this. These two models show significant errors, between 11% and 15% for the three surface roughness ratios and depending upon whether the TI or the TSS profiles are used to calculate the IBL heights from the LES results. The

Table 3 List of IBL models evaluated using the LES data

Author(s)	IBL Model
Elliott (1958)	$\delta_i = z_{02}\,[0.75 - 0.03\,\ln(1/m)]\,(x/z_{02})^{0.8}$
Wood (1982)	$\delta_i = 0.28\,[\max(z_{01}, z_{02})]\,[x/\max(z_{01}, z_{02})]^{0.8}$
Panofsky and Dutton (1984)	$\delta_i\left[\ln(\delta_i/z_{02}) - 1\right] + z_{02} = 1.25\,\kappa x$
Jegede and Foken (1999)	$\delta_i = 0.09\,(x)^{0.8}$
Savelyev and Taylor (2005)	$\delta_i\left[\ln(\delta_i/z_{01}) - 1\right] = 1.25\,\kappa x[1 + 0.1\,\ln(1/m)]$

model by Panofsky and Dutton (1984) shows similar under-prediction beyond $x/\delta \approx 2.5$ for $m = 83.3$ and 125 but shows good agreement throughout the domain for $m = 20$. This model is accurate for $m = 20$ (errors less than 6%) but not for the larger values of m (errors more than 10%). In contrast, the Elliott (1958) model shows overall good agreement for the larger two values of m (errors less than roughly 7%) but shows a significant over-prediction for $m = 20$ (error around 20%). The model by Savelyev and Taylor (2005) shows small over-predictions before, and small under-predictions after, $x/\delta \approx 2.5$ for $m = 83.3$ and 125, and small over-predictions throughout the domain for $m = 20$. The error norms are almost always less than 10%, so this model provides reasonable accuracy over a range of m values.

Table 4 Norms of the differences between IBL model predictions and the IBL heights obtained from LES. The IBL heights are calculated based on either the TSS (left panel) or the TI (right panel) profiles from the LES results

	δ_i LES based on TSS			δ_i LES based on TI		
IBL Model	$m = 20$	$m = 83.3$	$m = 125$	$m = 20$	$m = 83.3$	$m = 125$
Elliot	17.5%	7.6%	7.1%	21.0%	5.8%	6.1%
Wood	14.8%	14.1%	11.3%	11.3%	13.5%	12.7%
Jegede-Foken	15.5%	14.8%	12.0%	12.1%	14.2%	13.4%
Panofsky-Dutton	7.0%	11.8%	10.6%	3.6%	11.2%	12.3%
Savelyev-Taylor	9.5%	8.1%	8.1%	10.8%	6.9%	8.7%

3.5 Model for Turbulence Intensity

Development of an analytical model for the turbulence intensity downstream of a step change in surface roughness is pursued in this section. To motivate the idea, Fig. 16 shows the TI profiles at different distances downstream of the surface roughness jump along with the profile averaged over the upstream portion. Further, the gray dashed line in Fig. 16 represents the TI profile obtained

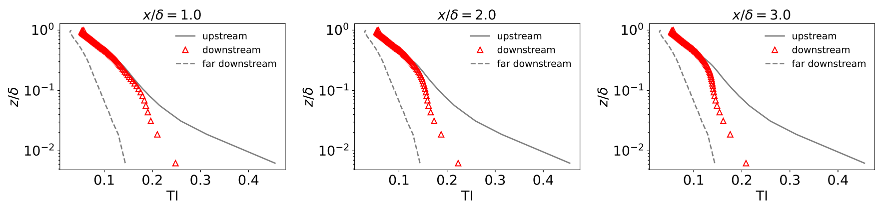

Fig. 16 Vertical profiles of TI at different downstream locations for $m = 83.3$ using the APA wall model compared with profiles in the upstream region and at far-downstream locations on grid G3

from a simulation of the flow over a homogeneous surface with roughness z_{02} (i.e. with the same surface roughness as in the downstream portion of the heterogeneous case). This simulation is henceforth denoted as 'far-downstream', since it is expected that at sufficiently far downstream of the roughness jump, the flow would have adjusted fully to the new surface conditions (roughness z_{02}) and would have no imprint of the abrupt roughness transition. It is observed that as the downstream distance changes from $x/\delta = 1$ to 3, the TI profile gradually departs from the upstream profile and approaches the far-downstream profile.

The observation in Fig. 16 that the TI profiles downstream of the roughness jump are bounded by the upstream and far-downstream TI profiles is utilized to develop a simple analytical model for the TI. The TI at a downstream location can be expressed as a weighted average of the upstream and far-downstream TI profiles,

$$TI(x,z) = \phi\, TI_{\text{far-downstream}} + (1-\phi)\, TI_{\text{upstream}}, \tag{13}$$

which can be arranged as

$$\phi(x,z) = \frac{TI(x,z) - TI_{\text{upstream}}(z)}{TI_{\text{far-downstream}}(z) - TI_{\text{upstream}}(z)}. \tag{14}$$

In the above equation, $TI_{upstream}$ and $TI_{far-downstream}$ are not evolving with the streamwise distance and are functions only of z since they come from simulations of flow over homogeneously rough surfaces with roughnesses z_{01} and z_{02} respectively. The empirical, reverse-logarithmic-law model (Stevens et al. 2018) can be easily used for these two quantities in place of the simulation results.

Figure 17a shows vertical profiles of $\phi(x,z)$ extracted from our LES results using Eq. 14 at representative downstream locations of $x/\delta = 1, 2$ and 3 for $m = 83.3$. As expected, ϕ is bounded between 0 and 1. A phenomenological model is developed for the weighting function considering it to be dependent on the downstream distance x and the IBL height $\delta_i(x)$,

$$\phi_{MODEL} = \sqrt{C\,\frac{\ln\left(z/\delta_i(x)\right)}{\ln\left(\delta_e(x)/\delta_i(x)\right)}}, \tag{15}$$

Equation 15 ensures that ϕ_{MODEL} goes to 0 at $z = \delta_i$ and to C at $z = \delta_e$. For the current study a value of $C = 0.8$ is taken. A further correction is required

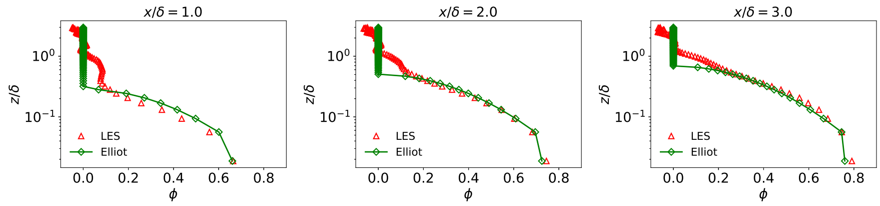

(a) ϕ

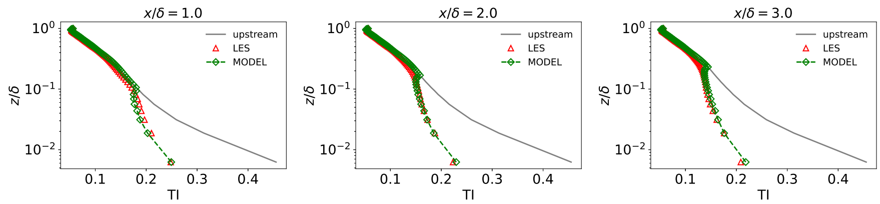

(b) TI

Fig. 17 Comparison of LES results on grid G3 for $m = 83.3$ at different downstream locations of (a) weighting function ϕ and (b) TI to model predictions. Model for ϕ is Eq. 15 and for TI is Eq. 13. In each model, δ_i is obtained using Elliot's relation

at the first vertical point from the wall, as this point is heavily influenced by the wall model in the LES simulations. Equation 15 is multiplied by 0.85 at the first computational point from the wall. To close this model, we use the Elliott (1958) relation for specifying the IBL height and set $\alpha = \delta_e/\delta_i = 0.027$, consistent with the value used for the APA wall model.

Figure 17a shows that this model for ϕ is in fair agreement with the LES results. In particular, the variation of ϕ with height below the IBL height is captured well by the model for all downstream locations. Using this modelled profile for ϕ in Eq. 13 gives a model for TI downstream of a step change in surface roughness.

Comparisons between the LES results and the model predictions are shown in Fig. 17b. It is clear that the proposed model predicts the TI very well at different downstream locations. The modelled TI profile shows a small kink near the top of the IBL, but the agreement with the LES results over the major portion of the domain is very good. The maximum relative error between the LES results and model predictions for TI is 4% close to the top of the IBL.

The model is tested against LES data for other roughness ratios as presented in Fig. 18 at a downstream location of $x/\delta = 3.0$. The profiles of ϕ and TI from the model are seen to be in good agreement with the LES results for these cases as well, indicating that the framework developed here is applicable for a range of surface roughness ratios.

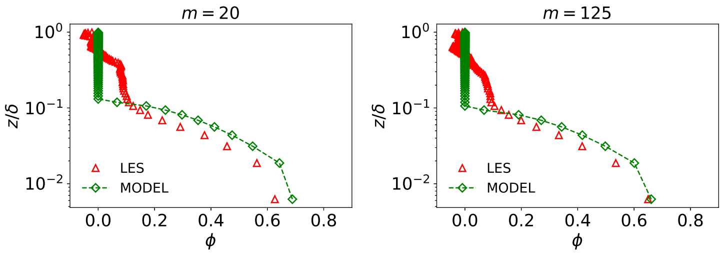

(a) ϕ

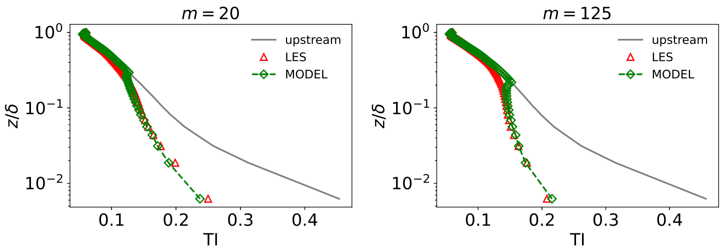

(b) TI

Fig. 18 Comparison of LES results on grid G3 for different values of m at downstream location $x/\delta = 3$ of (a) weighting function ϕ and (b) TI to model predictions. Model for ϕ is Eq. 15 and for TI is Eq. 13. In each model, δ_i is obtained using Elliot's relation

Sensitivity of the model for the turbulence intensity to the choice of IBL height model is shown in Fig. 19. Table 5 shows the maximum relative error between the TI predicted by model using different IBL models and the LES results. Using either the Panofsky and Dutton (1984) model or the Savelyev and Taylor (2005) model for the IBL height leads to fairly good predictions of the turbulence intensity profiles at different downstream locations for all three roughness ratios studied here. The kink close to the IBL height is more pronounced when the IBL height is modelled using the relations proposed by Panofsky and Dutton (1984) and is smallest on using the Elliott (1958) relation.

Table 5 Maximum error between the TI at $x/\delta = 3.0$ obtained from LES for different values of m and model predictions of TI using three different IBL models

IBL model	$m = 20$	$m = 83.3$	$m = 125$
Elliot	5.8%	4.0%	5.0%
Panofsky-Dutton	3.9%	8.9%	9.2%
Savelyev-Taylor	3.9%	6.0%	6.9%

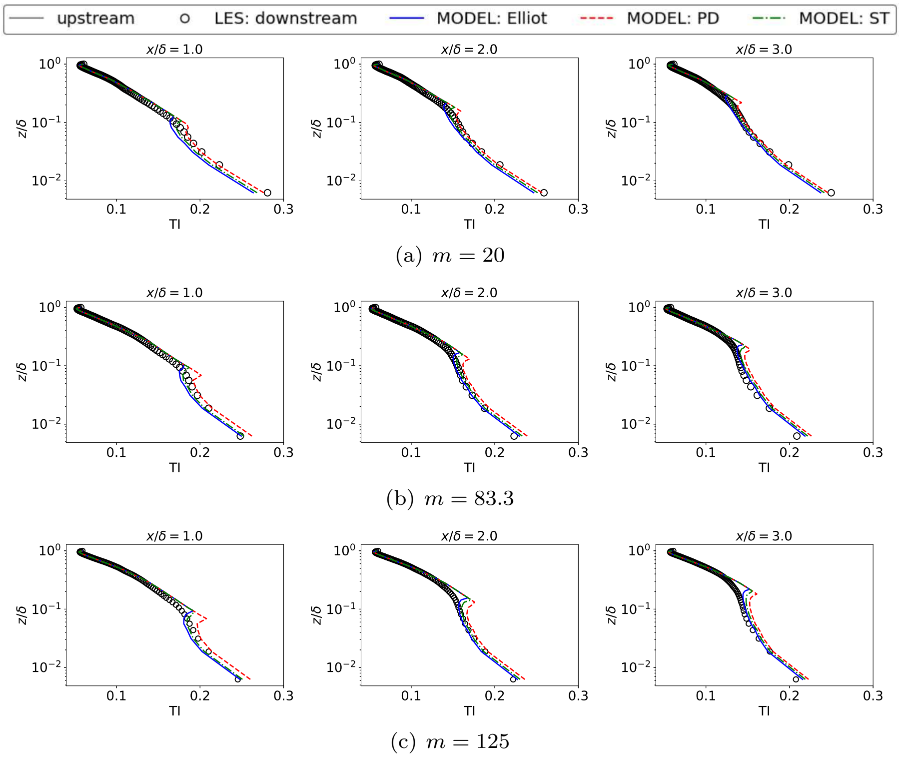

Fig. 19 Comparison of LES results on grid G3 at different downstream locations for (a) $m = 20$, (b) $m = 83.3$ and (c) $m = 125$ of TI to model predictions, Eq. 13, with ϕ given by Eq. 15 and δ_i obtained using three different IBL models, Elliott, Panofsky-Dutton (PD) and Savelyev-Taylor (ST)

4 Conclusion

The flow over a heterogeneously rough surface, with an abrupt change in the aerodynamic roughness, is studied here using large eddy simulations. Simulations are carried out using two wall models (BZ and APA), three ratios of the upstream to downstream roughness ($m = z_{01}/z_{02}$), different grid sizes and different values of the ratio $\alpha = \delta_e/\delta_i$, which is an input to the APA wall model. The LES data are compared with appropriate results from the previously reported wind-tunnel experiments of Chamorro and Porté-Agel (2009) and Li et al. (2021).

Different turbulent statistics of the ABL flow are found to be sensitive to the wall models to different extents. Specifically, the wall shear stress and turbulence intensity (TI) profile show a large sensitivity to the wall model, with the APA model giving larger values for both, and being in better agreement with the experimental results. The mean velocity profile is affected by the wall model to a lesser extent while the profile of the total shear stress (TSS) is almost insensitive to the wall model except for very close to the bottom wall. The internal boundary layer height, defined as the height above the bottom surface above which the upstream and downstream profiles are the same, is largely insensitive to the wall model as well as to the quantity (either TSS or TI) used to define it.

The LES results on using the APA model are dependent on the ratio, α, of the equilibrium boundary layer height to the internal boundary layer (IBL) height. Our results show that for the roughness ratios considered herein, the APA model predictions agree well with the experiments when $\alpha = 0.027$, i.e. when the equilibrium boundary layer height is 2.7% of the IBL height.

The sensitivity of the flow to changing downstream surface roughness is studied. As the value of m is increased, the downstream surface becomes more smooth and exerts lesser drag force on the flow. This leads to smaller surface shear stresses and turbulence intensities as well as to larger acceleration of the flow close to the wall. The IBL heights calculated based on TSS and TI profiles are found to be independent of the surface roughness ratio. Different analytical models for the IBL height evolution are evaluated. The widely-used Elliott (1958) empirical relation is found to be accurate for higher values of m, but is found to over-predict the IBL heights for the smallest m studied here. The model proposed by Panofsky and Dutton (1984) is found to be accurate for the smallest m but under-predicts the results for larger m. The Savelyev and Taylor (2005) model is found to be in reasonable agreement with the LES results for the IBL height for all values of m studied here.

An analytical model is proposed for the turbulence intensity downstream of the surface roughness jump. This model predicts the TI as a weighted average between the upstream TI profile and the TI profile far downstream of the surface roughness jump. The weighting function, $\phi(x, z)$, is determined by a simple relation and requires the IBL height as an input. Reasonably accurate predictions for the TI are obtained on using any of the three models mentioned above for the IBL height. Nominally, the IBL height given by the Elliott (1958) relation gives good prediction of the turbulence intensity at all downstream locations and for all surface roughness values studied here.

The work presented in this paper can be extended along several directions. More experiments and/or wall-resolved LES at surface roughness ratios greater than $m = 83.3$ need to be carried out that will enable development of a methodology of specifying the input α to the APA wall model for these large roughness ratios. The work here focused only on rough-to-smooth transition, and can be extended to smooth-to-rough transitions as well. Finally, studies of surface heterogeneities in the presence of other features, such as a hill, or one or more wind turbines, as well as other configurations of surface roughness heterogeneities can also be carried out.

Acknowledgements NSG thanks the IIT Hyderabad institute seed grant and SERB Startup Research Grant (SRG/2020/000265) for enabling this work as well as computational resources made available under the National Supercomputing Mission on Param-Brahma at IISER Pune (Grant DST/NSM/R&D_HPC_Applications/2021/28).

References

Abkar M, Porté-Agel F (2012) A new boundary condition for large-eddy simulation of boundary-layer flow over surface roughness transitions. Journal of Turbulence 13:N23

Abkar M, Bae HJ, Moin P (2004) Turbulent flows over rough walls. Annual Review of Fluid Mechanics 36:173–196

Abkar M, Bae HJ, Moin P (2016) Minimum-dissipation scalar transport model for large-eddy simulation of turbulent flows. Physical Review Fluids 1(4):041,701

Albertson JD, Parlange MB (1999) Surface length scales and shear stress: Implications for land-atmosphere interaction over complex terrain. Water Resources Research 35(7):2121–2132

Anderson W (2020) Turbulent channel flow over heterogeneous roughness at oblique angles. Journal of Fluid Mechanics 886:A15

Anderson W, Meneveau C (2010) A large-eddy simulation model for boundary layer flow over surfaces with horizontally resolved but vertically unresolved roughness elements. Boundary-Layer Meteorology 137:397–415

Anderson W, Meneveau C (2011) Dynamic roughness model for large-eddy simulation of turbulent flow over multiscale, fractal-like rough surfaces. Journal of Fluid Mechanics 679:288–314

Anderson W, Barros JM, Christensen KT, Awasthi A (2015) Numerical and experimental study of mechanisms responsible for turbulent secondary flows in boundary layer flows over spanwise heterogeneous roughness. Journal of Fluid Mechanics 768:316–347

Antonia R, Luxton R (1971) The response of a turbulent boundary layer to a step change in surface roughness part 1. smooth to rough. Journal of Fluid Mechanics 48(4):721–761

Antonia R, Luxton R (1972) The response of a turbulent boundary layer to a step change in surface roughness. part 2. rough-to-smooth. Journal of Fluid Mechanics 53(4):737–757

Bou-Zeid E, Meneveau C, Parlange MB (2004) Large-eddy simulation of neutral atmospheric boundary layer flow over heterogeneous surfaces: Blending height and effective surface roughness. Water Resources Research 40(2):W02,505

Bou-Zeid E, Anderson W, Katul GG, Mahrt L (2020) The persistent challenge of surface heterogeneity in boundary-layer meteorology: a review. Boundary-Layer Meteorology 177(2):227–245

Bradley EF (1968) A micrometeorological study of velocity profiles and surface drag in the region modified by a change in surface roughness. Quarterly Journal of the Royal Meteorological Society 94(401):361–379

Brasseur J, Wei T (2010) Designing large-eddy simulation of the turbulent boundary layer to capture law-of-the-wall scaling. Physics of Fluids 22:021,303

Chamorro LP, Porté-Agel F (2009) Velocity and surface shear stress distributions behind a rough-to-smooth surface transition: a simple new model.

Boundary-layer meteorology 130(1):29–41

Efros V, Krogstad PÅ (2011) Development of a turbulent boundary layer after a step from smooth to rough surface. Experiments in fluids 51(6):1563–1575

Elliott WP (1958) The growth of the atmospheric internal boundary layer. Eos, Transactions American Geophysical Union 39(6):1048–1054

Garratt JR (1994) The atmospheric boundary layer. Earth-Science Reviews 37(1-2):89–134

Ghaisas NS (2020) A predictive analytical model for surface shear stresses and velocity profiles behind a surface roughness jump. Boundary-Layer Meteorology 176(3):349–368

Ghaisas NS, Archer CL, Xie S, Wu S, Maguire E (2017) Evaluation of layout and atmospheric stability effects in wind farms using large-eddy simulation. Wind Energy 20:1227–1240

Ghaisas NS, Ghate AS, Lele SK (2020) Effect of tip spacing, thrust coefficient and turbine spacing in multi-rotor wind turbines and farms. Wind Energy Science 5(1):51–72

Ghate A, Towne A, Lele S (2020) Broadband reconstruction of inhomogeneous turbulence using spectral proper orthogonal decomposition and gabor modes. Journal of Fluid Mechanics 888

Ghate AS, Lele S (2020) Gabor mode enrichment in large eddy simulations of turbulent flow. Journal of Fluid Mechanics 903

Ghate AS, Lele SK (2017) Subfilter-scale enrichment of planetary boundary layer large eddy simulation using discrete fourier–gabor modes. Journal of Fluid Mechanics 819:494–539

Gul M, Ganapathisubramani B (2022) Development of turbulent boundary layers past a step change in wall roughness. Journal of Fluid Mechanics 947:A6

Hanson R, Ganapathisubramani B (2016) Development of turbulent boundary layers past a step change in wall roughness. Journal of Fluid Mechanics 795:494–523

Howland MF, Ghate AS, Lele SK, Dabiri JO (2020) Optimal closed-loop wake steering–part 1: Conventionally neutral atmospheric boundary layer conditions. Wind Energy Science 5(4):1315–1338

Jegede OO, Foken T (1999) A study of the internal boundary layer due to a roughness change in neutral conditions observed during the linex field campaigns. Theoretical and Applied Climatology 62(1):31–41

Khanna S, Brasseur J (1997) Analysis of Monin-Obukhov similarity from large-eddy simulation. Journal of Fluid Mechanics 345:251–286

Li M, de Silva CM, Rouhi A, Baidya R, Chung D, Marusic I, Hutchins N (2019) Recovery of wall-shear stress to equilibrium flow conditions after a rough-to-smooth step change in turbulent boundary layers. Journal of Fluid Mechanics 872:472–491

Li M, de Silva CM, Chung D, Pullin DI, Marusic I, Hutchins N (2021) Experimental study of a turbulent boundary layer with a rough-to-smooth change in surface conditions at high reynolds numbers. Journal of Fluid Mechanics 923:A18

Li M, de Silva CM, Chung D, Pullin DI, Marusic I, Hutchins N (2022) Modelling the downstream development of a turbulent boundary layer following a step change of roughness. Journal of Fluid Mechanics 949:A7

Moeng CH (1984) A large-eddy-simulation model for the study of planetary boundary-layer turbulence. Journal of the Atmospheric Sciences 41(13):2052–2062

Monin A, Obukhov A (1959) Basic laws of turbulent mixing in the ground layer of the atmosphere (osnovne zakonomernosti turbulentnogo peremeshivaniya v prizemnom sloe atmosfery). American Meteorological Society Boston MA, Tech rep

Munters W, Meneveau C, Meyers J (2016) Shifted periodic boundary conditions for simulations of wall-bounded turbulent flows. Physics of Fluids 28(2):025,112

Panofsky HA, Dutton JA (1984) Atmospheric turbulence: Models and methods for engineering applications. Models and methods for engineering applications 1st ed.

Panofsky HA, Townsend A (1964) Change of terrain roughness and the wind profile. Quarterly Journal of the Royal Meteorological Society 90(384):147–155

Plate E, Hidy G (1967) Laboratory study of air flowing over a smooth surface onto small water waves. Journal of Geophysical Research 72(18):4627–4641

Rao K, Wyngaard J, Coté O (1974) The structure of the two-dimensional internal boundary layer over a sudden change of surface roughness. Journal of Atmospheric Sciences 31(3):738–746

Rozema W, Bae HJ, Moin P, Verstappen R (2015) Minimum-dissipation models for large-eddy simulation. Physics of Fluids 27(8):085,107

Savelyev SA, Taylor PA (2005) Internal boundary layers: I. height formulae for neutral and diabatic flows. Boundary-Layer Meteorology 115(1):1–25

Shir C (1972) A numerical computation of air flow over a sudden change of surface roughness. Journal of Atmospheric Sciences 29(2):304–310

Sridhar A, Pullin D, Cheng W (2017) Rough-wall turbulent boundary layers with constant skin friction. Journal of Fluid Mechanics 818:26–45

Stevens RJ, Graham J, Meneveau C (2014) A concurrent precursor inflow method for large eddy simulations and applications to finite length wind farms. Renewable energy 68:46–50

Stevens RJAM, Martinez-Tossas LA, Meneveau C (2018) Comparison of wind farm large eddy simulations using actuator disk and actuator line models with wind tunnel experiments. Renewable Energy 116:470–478

Stull RB (1988) An Introduction to Boundary Layer Meteorology. Springer Dordrecht

Subramaniam A, Ghate A, Ghaisas NS, Howland MF, et al. (2021) PadeOps GitHub Repository

Taylor P (1969) On wind and shear stress profiles above a change in surface roughness. Quarterly Journal of the Royal Meteorological Society 95(403):77–91

Vreugdenhil CA, Taylor JR (2018) Large-eddy simulations of stratified plane couette flow using the anisotropic minimum-dissipation model. Physics of Fluids 30(8):085,104

Wood D (1982) Internal boundary layer growth following a step change in surface roughness. Boundary-Layer Meteorology 22(2):241–244

Xie S, Ghaisas NS, Archer CL (2015) Sensitivity Issues in Finite-Difference Large-Eddy Simulations of the Atmospheric Boundary Layer with Dynamic Subgrid-Scale Models. Boundary-Layer Meteorology 157:421–445

Zahiri AP, Roohi E (2019) Anisotropic minimum-dissipation (amd) subgrid-scale model implemented in openfoam: Verification and assessment in single-phase and multi-phase flows. Computers & Fluids 180:190–205